ASCE

Two-Scale Discrete Element Modeling of Gyratory Compaction of Hot Asphalt

Teng Man[1]; Jia-Ling Le, M.ASCE[2]; Mihai Marasteanu[3]; and Kimberly M. Hill[4]

Abstract: This paper presents a discrete element model for simulations of the compaction process of hot mixed asphalt (HMA). The model is anchored by the concept of a fine aggregate matrix (FAM), which consists of the binder and fine aggregates. In the simulation, the coarse aggregates are explicitly modeled as composite particles. Meanwhile, the FAM is considered as the thick coating of the coarse aggregates with complex constitutive laws. Interparticle interactions include influences of (1) particle properties via Hertz–Mindlin relations; and (2) FAM properties via lubrication relationships. The lubrication relationships include a variable for viscosity for which we derive normal and tangential rate-dependent forms using rheology theory of dense granular-fluid systems, verified reasonable for our systems with the discrete element simulations and experiments with FAM. We assimilate these elements into gyratory compaction simulations of HMA of different aggregate size distributions. We compare these with experiments and find that this model is capable of capturing the measured effects of grain size distribution on the overall compaction behavior of HMA. We conclude by highlighting the advantages of this discrete element model for HMA compaction problems. **DOI: 10.1061/(ASCE)EM.1943-7889.0002033.**

Introduction

More than 90% of paved roads in the United States are made of asphalt mixtures. There has been a sustained interest in improving the resilience and durability of asphalt pavements. It is widely accepted that the performance of asphalt pavements is strongly influenced by the material porosity, which is governed by the compaction process. Undercompacted asphalt mixtures would exhibit a high air void ratio and low material strength. On the other hand, overcompacted asphalt mixtures would be susceptible to high-temperature sensitivity (Ricardo-Archilla and Madanat 2001). Therefore, understanding the compaction process of asphalt mixtures is a critical subject of research in asphalt pavements. However, as compared to the extensive effort on modeling the mechanical behavior of asphalt mixtures, studies have focused on physics-based modeling of the compaction of hot mix asphalt (HMA).

The existing modeling efforts on compaction of asphalt mixtures can be generally divided into two categories, i.e., continuum-based and discrete-based models. Guler et al. (2004) proposed a modified porous elastoplastic model to simulate the deformation of HMA during the compaction process. In this model, the evolution of deformation arises primarily from plasticity and change of porosity while the viscous behavior of the asphalt binder was not explicitly considered. In a recent study, a thermodynamics-based visco-plastic constitutive model was developed, and the viscous effect of asphalt binder was taken into account (Koneru et al. 2008; Masad et al. 2016a, b). The model was calibrated using the Superpave gyratory compaction tests and was then used to predict the field compaction of HMA. The macroscopic continuum models offer an efficient numerical tool for large-scale simulations of the overall deformation of HMA during the compaction process. However, these models largely rely on phenomenological constitutive laws, which cannot explicitly capture the effect of individual material constituents on the compaction behavior of HMA. Therefore, continuum models are unable to predict the effect of particle-scale features of the asphalt mixtures, such as the aggregate size distribution, aggregate shape, and binder viscosity, on the overall compaction process.

In contrast to continuum models, the discrete element model (DEM) offers the unique advantage of its capability to explicitly model individual aggregates and in so doing captures some essential particle-scale features that influence the overall compaction process. In earlier attempts to use the DEM to model the asphalt compaction, the asphalt mixtures were treated as an assembly of dry particles and the interparticle interaction was described by the Hertz–Mindlin contact law alone (Wang et al. 2007). In recent DEM simulations of Superpave gyratory compaction and the vibratory compaction (Chen et al. 2012, 2014), Chen et al. used the Burger contact law characterized by mechanical tests of asphalt mastic to describe the forces between aggregates. In their study, when two particles were in contact, the interactions between them were calculated based on Burger's model of asphalt mastic, which ignored the elastic contact of solid aggregates themselves. The results underpredicted the air void ratio for a given compaction effort.

One might gain a more theoretical perspective of the HMA compaction process by considering the HMA as a particle assembly with a viscous interstitial fluid. Over the past decades, extensive efforts have been directed toward investigating the compaction behavior of particle assemblies under tapping excitation, vibration, or cyclic shearing (Nicolas et al. 2000; Luding et al. 2000; Pouliquen et al. 2003; Mehta et al. 2004). Previous research has focused on the

[1]Postdoctoral Research, Key Laboratory of Coastal Environment and Resources of Zhejiang Province (KLaCER), School of Engineering, Westlake Univ., Hangzhou, Zhejiang, China. ORCID: https://orcid.org/0000-0001-7912-7300

[2]Professor, Dept. of Civil, Environmental, and Geo-Engineering, Univ. of Minnesota, Minneapolis, MN 55455. ORCID: https://orcid.org/0000-0002-9494-666X

[3]Professor, Dept. of Civil, Environmental, and Geo-Engineering, Univ. of Minnesota, Minneapolis, MN 55455.

[4]Associate Professor, Dept. of Civil, Environmental, and Geo-Engineering and St. Anthony Fall Laboratory, Univ. of Minnesota, Minneapolis, MN 55455 (corresponding author). ORCID: https://orcid.org/0000-0002-2080-9793. Email: kmhill@umn.edu

Note. This manuscript was submitted on April 15, 2021; approved on August 30, 2021; published online on November 23, 2021. Discussion period open until April 23, 2022; separate discussions must be submitted for individual papers. This paper is part of the ***Journal of Engineering Mechanics***, © ASCE, ISSN 0733-9399.

particle-scale analysis of particle assemblies subjected to tapping and vibration that suggested theoretical relationships between collective particle-scale rearrangements and the compaction dynamics (Mehta et al. 2004; Pouliquen et al. 2003). Some other research investigated the compaction behavior under shearing excitation that more closely resembles the gyratory compaction of asphalt mixtures (Nicolas et al. 2000; Luding et al. 2000). Experimental investigations such as these have given rise to a physical intuition and understanding as well as theoretical expressions for the compaction process. For example, Knight et al. (1995) proposed a logarithmic relationship between the compaction cycles and the solid fraction of the particle assemblies under tapping excitation. This empirical expression was motivated by experimental data showing slow relaxation at early times followed by a near-steady state compaction level at long times. Others demonstrated that the logarithmic compaction relationship can be derived using a free volume model (Nowak et al. 1998) that assumes an exponential law for the rate evolution of the material density or a one-dimensional discrete lattice model (Peng and Ohta 1998). A subsequent study demonstrated that the logarithmic rate dependence of compaction also represents compaction under simple shearing of particle assemblies (Hartley and Behringer 2003).

In the paper, we present a discrete element computational model for the compaction of asphalt mixtures. For each mix, we consider aggregates smaller than 2.36 mm as fine aggregates and the rest as coarse aggregates. Inspired by recent research on two-scale DEM simulation of fracture of asphalt mixtures (Le et al. 2018), we balance the efficiency and accuracy of the computation by formulating our compaction DEM model at two scales. On the macroscopic level, only coarse aggregates are modeled by nonspherical particles. The interaction formulation between these aggregates uses two aspects: (1) contact theory between solid particles; and (2) lubrication theory to describe how the liquid-like mixture of asphalt binder and fine aggregates, hereinafter called fine aggregate matrix (FAM), modifies these interactions. As detailed shortly, we use small-scale simulations to calibrate a previously proposed relationship for the rheology of FAM for input parameters to the lubrication part of coarse particle interactions. As we describe in detail in the next sections, we use our model to simulate the gyratory compaction process of HMA of different aggregate size distributions.

Model Description

Introduction to an Efficient DEM Approach

The salient feature of the DEM is its ability to explicitly represent the particle properties and particle-scale rearrangements in large conglomerations of discrete elements. However, the computational cost increases dramatically as the number of particles (Minneapolis, Minnesota) increases (as $N \cdot ln(N)$), which is particularly problematic for systems of such wide grain size distributions with significant contributions of small particles as is true of HMA. In fact, for the number of particles present even for a relatively small HMA laboratory test, the high computational cost makes such a simulation essentially cost-prohibitive. To address this, Chen et al. (2012, 2014) explicitly modeled macroscopic particles using DEM while representing the finest particle and additives mixed with asphalt binder. They modeled the interparticle combined contact/particle-suspension forces through Burger's model. While it captured certain details of the phenomenology, it did not allow for the direct input of properties such as fluid viscosity or particle elasticity and required experimental fitting for the model parameters. A recent study on a similar system of *hardened* asphalt mixtures modeled the solid-like system by prescribing a minimal aggregate size to represent explicitly in the DEM. They proposed a two-scale DEM for simulations of low-temperature fracture of asphalt mixtures (Le et al. 2018, 2020). In the model, the asphalt mixture was represented by an assembly of coarse aggregates and the contact between these aggregates represented the FAM. The constitutive behavior of the interparticle contacts was determined by bending beam experiments on FAM. The results indicate that the DEM could predict the low-temperature fracture behavior of asphalt mixtures (Le et al. 2018).

Motivated by this recent work, for HMA gyratory compaction, we represent only the coarse aggregates in the DEM. Then, we develop a model interparticle interaction to represent forces between the coarse aggregates as it is mediated by the mixture of the smaller particles and finer materials in the asphalt binder. In other words, while the coarse particles may exert forces on one another through direct contact in our model, they may additionally exert forces on one another via the slurry-like mix of finer particles, bitumen, and other parts of the mixture. We use the concept of FAM from the literature (Caro et al. 2010; Graziani et al. 2020) to represent essentially everything else in the mixture aside from some parts of the air void. We envision this similarly to the fine aggregate (passing to the 2 mm sieve), filler, asphalt binder, and other filler materials.

In the model we describe herein, we represent the coarse aggregates as composite particles (particles consisting of two spheres linked with both normal and tangential springs). We determine the size distribution of these simulated particles according to the size distribution obtained from the sieve analysis of our physical materials. We treat the rest of the material as a single-phase mixture, i.e., we treat the FAM as an interstitial granular-fluid system.

Interaction Law between Particles

As is typical, we track all coarse aggregates at each time step in our DEM simulation. Thus, the majority of modeling work is in representing forces between these particles and how the presence of the FAM coating affects this interaction. We do so by representing the interaction between coarse aggregates with two types of forces: (1) forces activated when particles are deformed and thus associated with the particle materials themselves; and (2) forces associated with viscous resistance to flow of the FAM associated with properties of the slurry, binder, fine particles, and additives.

The force associated with deformation of contacting particles (i and j) is calculated by using the Hertz–Mindlin contact model as described by Tsuji et al. (1992) (Fig. 1), i.e.:

$$F_c^{ij,n} = -k_n\delta_n^{1.5} - c_n\delta_n^{0.25}\dot{\delta}_n \tag{1a}$$

$$F_c^{ij,t} = \min(-k_t\delta_n^{0.5}\delta_t - c_t\delta_n^{0.25}\dot{\delta}_t, \mu_p|F_c^{ij,n}|) \tag{1b}$$

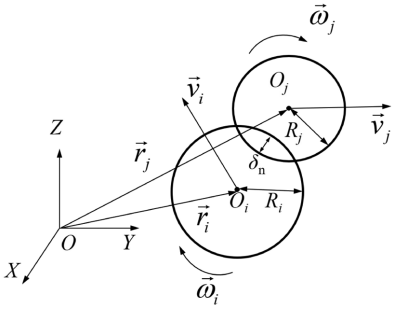

Fig. 1. Contact kinematics of two particles.

J. Eng. Mech., 2022, 148(2): 04021140

Table 1. Stiffness and damping parameters of the Hertz–Mindlin contact model

Model parameters	Expressions
k_n	$(4/3)\sqrt{R_{\text{eff}}}E_{\text{eff}}$
k_t	$8\sqrt{R_{\text{eff}}}G_{\text{eff}}$
c_n	$\alpha_d\sqrt{m_{\text{eff}}k_n}$ (α_d = constant)
c_t	$\alpha_d\sqrt{m_{\text{eff}}k_t}$ (α_d = constant)
R_{eff}	$(1/R_i + 1/R_j)^{-1}$
E_{eff}	$[(1-\nu_i^2)/E_i + (1-\nu_j^2)/E_j]^{-1}$
G_{eff}	$[2(1+\nu_i)(2-\nu_i)/E_i + 2(1+\nu_j)(2-\nu_j)/E_j]^{-1}$
m_{eff}	$(1/m_i + 1/m_j)^{-1}$

Note: R_i, E_i, ν_i, m_i = radius, elastic modulus, Poisson ratio, and mass of particle i, respectively.

where $F_c^{ij,n}$ and $F_c^{ij,t}$ = normal and tangential contact forces exerted on particle i by particle j, respectively. δ_n = model particle deformation represented, as is typical by $\delta_n = R_i + R_j - |\vec{r}_i - \vec{r}_j|$; where R_i and R_j = particle radii; and $\vec{r}_i$ and $\vec{r}_j$ = position vectors of two particles; δ_t = model tangential deformation at the contact point between two particles; and μ_p is the coefficient of friction. k_n, k_t are the normal and tangential stiffnesses, respectively; and c_n and c_t are the normal and tangential damping coefficients, respectively. The stiffnesses and damping coefficients are calculated according to the formulas in Table 1, in which α_d is determined from the coefficient of restitution (Tsuji et al. 1992; Hill and Tan 2014). Note that the magnitude of tangential contact force is limited by $\mu_p|F_c^{ij,n}|$, at which the two particles start to slide over each other.

We represent the resistive viscous forces of the FAM that coating the particles using lubrication theory (Goldman et al. 1967; Pitois et al. 2000; Liu et al. 2013; Marshall and Li 2014), i.e.:

$$F_b^{ij,n} = 6\pi\eta_n R_{\text{eff}}^2 \frac{\dot{\delta}_g}{\delta_g}\left\{1 - 1\Big/\sqrt{1 + \bar{V}/(\pi R_{\text{eff}}\delta_g^2)}\right\}^2 \tag{2a}$$

$$F_b^{ij,t} = 6\pi\eta_s R_{\text{eff}} v_t^{\text{rel}}\left[\frac{8}{15}\ln(R_{\text{eff}}/\delta_g) + 0.9588\right] \tag{2b}$$

where $F_b^{ij,n}$ and $F_b^{ij,t}$ = interparticle lubrication forces in the normal and tangential directions, respectively; δ_g = distance between the closest points on the surfaces of two particles as shown in Fig. 2(a); v_t^{rel} = tangential relative velocity between the adjacent particles; η_n, η_s = rate-dependent viscosities in the normal and shear directions, respectively, as we explain in Section 3. As an aside, typical derivation of the lubrication theory (Tsuji et al. 1992; Hill and Tan 2014) as well as its application usually involves isotropic Newtonian fluid coatings. Yet in this case, our coating—FAM—is a particle-fluid slurry that is neither isotropic nor Newtonian, as we discuss in Section 3. Before proceeding, we note that for high shear rates, there may be other fluid forces involved (e.g., (Trulsson et al. 2012). We suspect these to be minimal based on compaction gyration rates and pressure. Thus, we save these considerations for a future endeavor. To continue, in Eq. (2), δ_c is a representative average thickness of the FAM coating on the aggregates (Fig. 2); $\bar{V}$ is the effective volume of the interstitial FAM that is considered to contribute to the lubrication effect, which we estimate as $\bar{V} = 8\delta_c^3$, as shown appropriately in Ref. (Marshall and Li 2014).

We summarize the essential features of this framework as follows. First, when two neighboring particles are not so close that their FAM coatings overlap, i.e., $\delta_c < \delta_g$, the particles exert no force on one another, either directly or indirectly via lubrication forces. If $0 < \delta_g < \delta_c$, even though the particles are not directly touching, they effectively exert forces on one another via the viscous properties of the FAM coating. As we noted, the effective viscosities, η_n and η_s, are related to the mixture rheology of the FAM; and if $\eta_n \neq \eta_s$, the rheology of the FAM is anisotropic. As discussed in the next section, we determine the value of η_n and η_s through a rheology model for dense granular-fluid systems, which is informed by fine-scale DEM simulations. Fig. 2(b) shows a schematic of the relationship between the lubrication force and the interparticle distance for a constant relative velocity.

The overall dynamic equilibrium of the particle assembly is enforced by applying the Newton 2nd law to each particle. For particle i, we have the following set of equations:

$$m_i\frac{\mathrm{d}^2\vec{r}_i}{\mathrm{d}t^2} = \sum_{k=1}^{N_i}\left(\vec{F}_c^{ik,n} + \vec{F}_c^{ik,t} + \vec{F}_b^{ik,n} + \vec{F}_b^{ik,t}\right) \tag{3a}$$

$$J_i\frac{\mathrm{d}^2\vec{\theta}_i}{\mathrm{d}t^2} = \sum_{k=1}^{N_i}\left[\left(\vec{F}_c^{ik,t} + \vec{F}_b^{ik,t}\right) \times \left(R_i\vec{n}_{ik}\right)\right] \tag{3b}$$

where $\vec{r}_i$ = position vector of particle i; $\vec{\theta}_i$ = angular vector of rotation of particle i; R_i = radius of particle i; J_i = centroidal moment of inertia of particle i; N_i = number of particles that

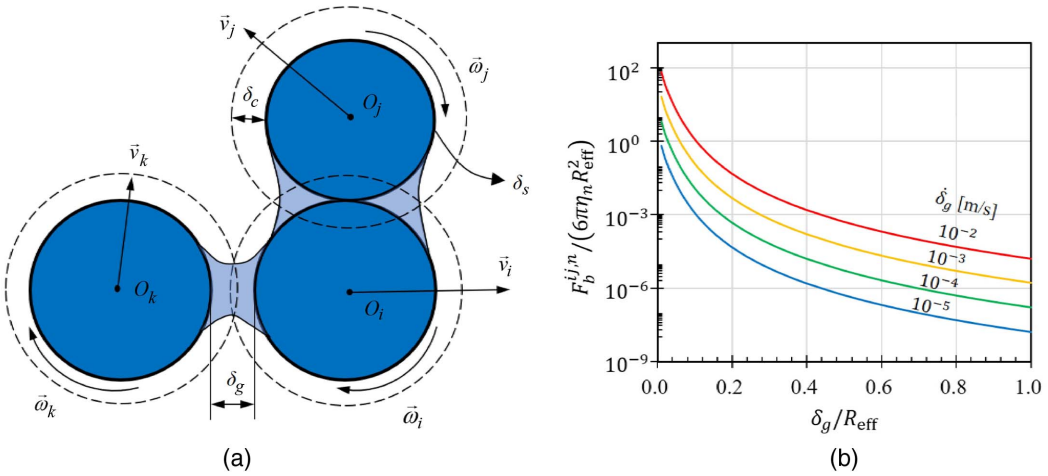

Fig. 2. Lubrication interaction between particles: (a) coated coarse aggregates surrounded by FAM; and (b) schematic plot of the relationship between lubrication force and particle distance for a fixed relative velocity.

J. Eng. Mech., 2022, 148(2): 04021140

are adjacent to particle i; and $\vec{n}_{ik}$ = unit vector connecting the centroids of particles i and k. The entire system of equations is solved by using the 4th order Runge–Kutta method.

Particle Asphericity: Composite Particle Model

Typical aggregates are irregularly shaped, unlike the spherical particles that would be most readily modeled as described by the force laws above. The most significant manner in which the particle asphericity can affect compaction is by arresting relative movement of neighboring particles through the interlocking of subparticle features. This interlock mechanism could have a considerable influence on compaction behavior. We represent this phenomenology by using a composite particle model. That is, we represent each nonspherical coarse aggregate with two spherical particles bonded together (Pöschel and Schwager 2005).

The bound particles have two different radii, one larger [particle m in Fig. 3(a)] and one smaller [particle n in Fig. 3(a)]. We locate the center of particle n on the surface of particle m. The nonsphericity S of a composite particle can be evaluated using the following equation:

$$S = 1 - \frac{L}{2R} \tag{4}$$

where $L = \max\{[1 + (R_n/R_m) + (\sqrt{2}/2)]R_m, 2R_m\}$ = minimal side-length of an enveloping square; $R = (1 + 0.5(R_n/R_m))R_m$ = minimal radius of an enveloping circle; and R_n, R_m = radii of particle m and n, respectively [Fig. 3(a)]. Fig. 3(b) shows the relation between S and R_n/R_m. In this study, we choose $R_n/R_m = 0.5$, which corresponds to $S = 0.117$.

To combine the two spheres to form a single particle, we assign both normal and tangential springs to connect the individual spheres (Pöschel and Schwager 2005). We consider the connection between particle m and n as an elastic beam with the cross section as the intersection of two particles (where the normal and tangential forces are calculated using the Hertz–Mindlin contact model except the overlap is replaced with the displacement between two particles. The moment between two particles is calculated based on Bernoulli beam theory with the beam cross section as a circle with radius $R_{\text{beam}} = R_n \sin[\cos^{-1}(0.5 \cdot R_n/R_m)])$ and the same beam length as the overlap between them ($L_{\text{beam}} = R_n$). While, when subjected to appropriate forces, the spheres move slightly relative to each other (normal displacement Δ_n, tangential displacement Δ_t, and angular displacement Δ_θ) and we could calculate the forces and moment

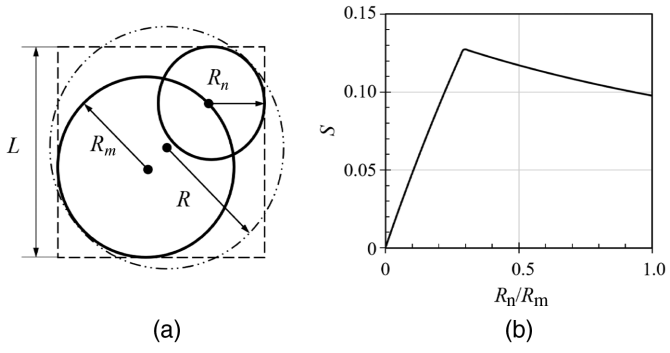

Fig. 3. Composite particle model: (a) nonspherical particle modeled by two spherical particles; and (b) relationship between nonsphericity and particle size ratio.

$$F_n^{m,n} = k_n \delta_n^{0.5} \Delta_n \tag{5a}$$

$$F_t^{m,n} = k_t \delta_n^{0.5} \Delta_t \tag{5b}$$

$$M^{m,n} = \frac{EI_{\text{beam}}}{L_{\text{beam}}} \Delta_\theta \tag{5c}$$

between them based on the connection beam we proposed so that the two connected particles are not allowed to slip relative to one another (Here, K_n and K_t are the normal and tangential stiffness and the ratio between them is a constant, and $I_{\text{beam}} = 0.25\pi R_{\text{beam}}^4$ is the moment of inertia of the beam cross section); and in this way, the composite particle can move as a single elastic body. The main advantage of the composite particle model is that the particle interaction can still be described by the aforementioned contact laws formulated for spherical particles (Zhao et al. 2015).

Fine-Scale DEM Simulations of Rheology of Fine Aggregate Matrix

As we discussed in Section 2, we calculate the lubrication forces between coarse aggregates based on the normal and tangential effective viscosities of the FAM, η_n, and η_s, though these are effectively unknown. Our approach is somewhat similar to that described in Chen et al. (2012, 2014), though in this previous work, they represented the behavior of asphalt binder and fillers through a Burger's interaction model that did not allow for direct input for constituent properties. Rather, their approach required experimental data with model parameter fitting. We strove to develop a model where we could directly input properties of our mixture constituents. To do this, we note that FAM is effectively a dense granular material with interstitial viscous fluid. Consequently, the rheology of FAM is fundamentally different from that of asphalt mastic. In this section, we describe a rheology model for FAM, guided by recent research on granular slurry rheology and informed by a set of fine-scale DEM simulations.

Based on numerical simulations and recent developments in particle-fluid flow behaviors, Trulsson et al. (2012) proposed that the average shear stress can be expressed in terms of a linear combination of theoretical collisional and viscous stresses:

$$\tau = f(\phi_s)[k\rho_s(\dot{\gamma}d_a)^2 + \eta_f\dot{\gamma}] \tag{6}$$

where τ = local averaged stream-wise shear stress; ϕ_s = solid fraction defined as the ratio between the volume of solid particles and the total volume of the system; ρ_s = density of the particles; d_a = average particle diameter; $\dot{\gamma}$ = shear rate; η_f = viscosity of the interstitial fluid; and k = fitting parameter.

We note that the relationship between $\mu_{\text{eff}} = \tau/\sigma_n$, where σ_n is the normal stress (or pressure) of the granular-fluid system, and $\dot{\gamma}$ is a characterization of the rheology of a granular system. If the system contains only dry particles, dimensional analysis (MiDi 2004; Forterre and Pouliquen 2008) suggests that μ_{eff} is dependent on the inertia number (MiDi 2004; Jop et al. 2006; Pouliquen et al. 2006):

$$I_c = \dot{\gamma}d_a/\sqrt{\sigma_n/\rho_s} \tag{7}$$

When the system contains interstitial fluid, recent analysis and experiments suggest that the rheology may exhibit a viscous-dominant behavior (Cassar et al. 2005; Trulsson et al. 2012). Boyer et al. (2011) proposed that in the viscous regime, the rheology of the granular system can be described by the viscous number

$$I_v = \eta_f\dot{\gamma}/\sigma_n \tag{8}$$

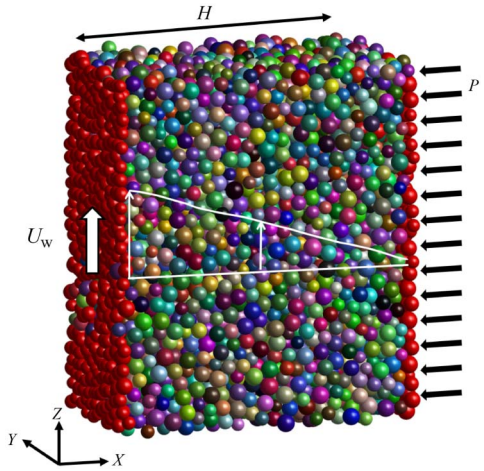

Fig. 4. DEM simulation of simple shear test of granular assembly in a Couette cell (the white line denotes a typical simulated velocity profile).

Trulsson et al. (Trulsson et al. 2012) recently suggested that we can describe the frictional rheology of a granular-fluid system by combining I_c and I_v into a single parameter K

$$K = I_v + kI_c^2 \tag{9}$$

K can be seen as a linear combination of Bagnold's theoretical collisional stress ($\tau_c \sim \rho_s(\dot{\gamma} d_a)^2$) (Bagnold 1954) and viscous stress ($\tau_v \sim \eta\dot{\gamma}$) normalized by the normal stress σ_n. Using 2D computational experiments, Trulsson et al. (2012) found they could express the effective frictional coefficient as

$$\mu_{\text{eff}} = \mu_{k1} + \frac{\mu_{k2} - \mu_{k1}}{1 + \sqrt{K_0/K}} \tag{10}$$

where μ_{k1}, μ_{k2}, and K_0 = fitting parameters.

To investigate the rheological properties of FAM, we perform a series of 3D DEM simulations of FAM in a 3D Couette cell under simple shear loading (Fig. 4). In the fine-scale DEM simulations, the particles have sizes uniformly distributed from $0.8d_a$ to $1.2d_a$, where $d_a = 2.5$ mm. We use the interparticle contact law described in the previous section, i.e., Eqs. (1), (2*a*), and (2*b*), where the viscosity of the interstitial fluid is directly used in the lubrication model ($\eta_n = \eta_s$). We set the interparticle frictional coefficient, $\mu_p = 0.1$ (Foerster et al. 1994). As in the previous section, we limit the lubrication effect to a maximum distance of $2\delta_c$, and a minimum distance of $0.1d_a$ corresponding to a roughness effect.

To shear these particles, we initiate a cell of a dimension of 30 mm in the $y-$ direction, 58.3 mm in the $z-$ direction, and the initial dimension in the $x-$ direction is 51.5 mm. We release particles in random configuration and begin to shear the cell as follows. We set periodic boundary conditions in the $y-$ and $z-$ directions. We assign the left vertical wall (in Fig. 4), what we refer to as the translational wall, a constant velocity U_w and restrain it from moving in the $x-$ and $z-$ directions. The right vertical wall is restrained in the $y-$ and $z-$ directions and assigned a constant pressure in the $x-$ direction. The right wall is allowed to only move in the $x-$ direction so that constant pressure can be maintained throughout the simulation. To initiate the experiments, we release particles in a random arrangement between the walls. To roughen the walls, we affix particles whose centroid is less than a certain distance (2.5 mm) to the walls. These particles move rigidly with the walls. From one experiment to the next, we systematically vary the velocity of the translational wall from 0.001 m/s to 10 m/s. We systematically vary pressure from 100 Pa to 1 kPa the viscosity of interstitial fluid from 0 to 2×10^5 cP.

During the simulation, the system experiences a simple shear loading driven by the motion of the translational wall. As the system reaches a steady state, which is manifested by a stabilized boundary shear stress, we obtain a linear velocity profile in the Couette cell shown in Fig. 4. The different sets of model parameters in the simulation correspond to a wide range of the inertia and viscous numbers: $I_c \in [10^{-3}, 1]$ and $I_v \in [10^{-7}, 1]$, which cover the relevant values of I_c and I_v for subsequent simulation of gyratory compaction of HMA.

Fig. 5(a) shows the simulated relationship between the effective frictional coefficient μ_{eff} and K, in which we choose $k = 0.03$ so that the data point could collapse onto one curve (Man 2019). The optimum fitting of the simulation results by Eq. (10) results in the following parameters: $\mu_{k1} = 0.265, \mu_{k2} = 2.2$, $K_0 = 0.25$. We note that the value μ_{k2} may be better determined if the simulation includes larger values of K. However, for the results we described here, this is inconsequential because our results cover a sufficient range for the compaction simulations, as we detail shortly.

Fig. 5(b) shows the simulated relationship between the solid fraction and K. Similar to Fig. 5, the simulation data collapse onto a single curve when we choose $k = 0.03$. The shape of the simulated $\phi_s - K$ curve can be approximated by the following equation (Man 2019):

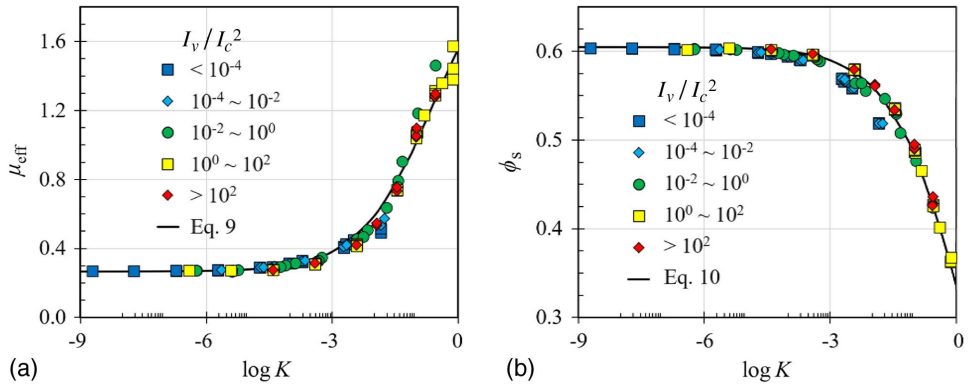

Fig. 5. (a) Simulated relationship between dimensionless number, $K = I_v + 0.03I_c^2$, and effective frictional coefficient, μ_{eff}, and its optimum fit by Eq. (10); and (b) relationship between K and solid fraction and its optimum fit by Eq. (11).

J. Eng. Mech., 2022, 148(2): 04021140

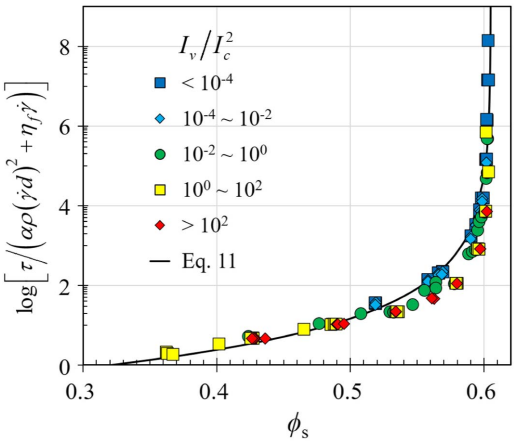

Fig. 6. Simulated relationship between normalized shear stress, $\tau/[\alpha\rho(\dot{\gamma}d)^2 + \eta_f\dot{\gamma}]$ and solid fraction ϕ_s and its optimum fit by Eq. (12).

$$\phi_s = \frac{\phi_m}{1+\beta_k\sqrt{K}} \tag{11}$$

where ϕ_m, β_k = constants. For an optimum fit of the $\phi_s - K$ curve [Fig. 5(b)], we find $\phi_m = 0.605$ and $\beta_k = 0.8$.

Using Eq. (6), we plot a normalized shear stress $\tau/[\alpha\rho(\dot{\gamma}d_a)^2 + \eta_f\dot{\gamma}]$ versus the solid fraction ϕ_s in Fig. 6. By fitting this relationship, we obtain function $f(\phi_s)$ in Eq. (6), i.e.:

$$f(\phi_s) = \frac{1}{26}(\phi_m - \phi_s)^{-2.52} \tag{12}$$

By combining Eqs. (10)–(12) with the fitted parameters, we can determine a rheology expressed as the effective viscosities η_n and η_s

$$\eta_s = \tau/\dot{\gamma} = 0.136(0.03\rho_s\dot{\gamma}d_a^2 + \eta_f)\left(1+\frac{1}{0.8\sqrt{K}}\right)^{2.52} \tag{13}$$

$$\eta_n = \eta_s\left\{0.265 + \frac{1.935}{1+\sqrt{0.25/K}}\right\}^{-1} \tag{14}$$

It is evident that the FAM exhibits a nonNewtonian behavior, in which the effective viscosities depend strongly on the local shear rate. Eqs. (13) and (14) are numerically implemented in an explicit manner in the DEM simulation of the whole mixture. In this model, after time step i, we have determined the particle positions, particle velocities, and particle interaction forces. As we proceed to the current time step, $i+1$, we first check the contact condition between two particles. If two particles are not physically in contact, we need to calculate only the lubrication forces. Otherwise, both the Hertz–Mindlin contact and lubrication forces need to be calculated. Based on Eqs. (1*a*) and (1*b*), the Hertz–Mindlin contact forces can be determined based on the overlap and relative velocities of the particles calculated from the previous time step. For the lubrication forces, we can obtain K from Eq. (11) based on the solid fraction of FAM and $\dot{\gamma}$ from the coarse particle velocities and particle distances. Through the present rheological model [Eqs. (13) and (14)], we determine the normal and tangential effective viscosities of the interstitial FAM and then obtain the new lubrication forces based on Eqs. (2*a*) and (2*b*). With all the updated interaction forces, we can solve the system of equilibrium equations to update the particle positions, velocities, and accelerations.

Experimental Investigation

To validate the proposed model for HMA, we performed a set of laboratory experiments and corresponding simulations. We used a Superpave gyratory compactor [Fig. 7(a)] to compact different asphalt mixtures. We used PG 64-22 asphalt binder and three sets of aggregates of different size distributions with similar median grain size (Table 2), as shown in Fig. 7(b). The median sizes of fine aggregate differed by approximately 10%, and the main difference in the FAM from one mixture to the next was the mass ratio of fine aggregates denoted by $\alpha_f = m_f/m_{ag}$. The binder viscosity we found to be approximately 250 cP at compaction temperature $T = 135$°C. We label the three mix designs as N30, N50, and N100, respectively, based on the results of the compaction test. Table 2 presents some detailed information of the aggregates used for these mixes.

Prior to our experiments, we placed the asphalt binders and aggregates in the oven at 140°C for 2 h and then we mix them in a lab mixer for 3 min. We placed the HMA in a Brovold Superpave gyratory compactor for the compaction experiment according to ASTM D6925 (ASTM 2015). The gyratory compactor we used consists of a cylindrical gyratory ring, loading plate, and gyratory plate [Fig. 7(a)]. During the compaction process, the bottom plate moves vertically under a constant pressure; for our experiments, we set the pressure at 600 kPa. At the same time, we set the top plate to gyrate horizontally with a gyratory speed of 30 rpm. Our cylindrical container/ring was set with a gyratory angle of 1.25° which leads to the gyratory motion of the cylindrical ring to produce the macroscopic average shear rate of approximately 0.07/s.

During the compaction test, we tracked the position of the bottom plate at the rate of once per gyration. At the end of the compaction test, we measured the bulk specific gravity of the mix, G_{mb}, according to ASTM D2726 (ASTM 2019). Meanwhile, we

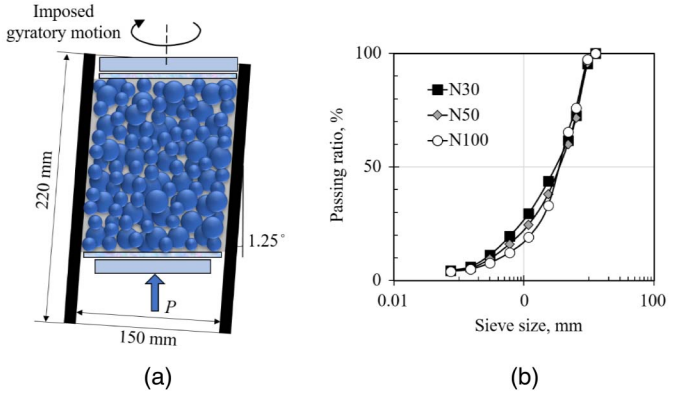

Fig. 7. Gyratory compaction experiments: (a) configuration of the Superpave gyratory compactor; and (b) grain size distribution of aggregates.

Table 2. Mix design of the experiments, characteristic parameters of the grain size distribution of aggregates

Test	Asphalt binder	Binder ratio	Binder viscosity, η_f (cP)	Median aggregate size, d_{50} (mm)	$\alpha_f = m_f/m_{ag}$	d_a (mm)
N30	PG64-22	5.5%	250	3.20	0.437	0.530
N50	PG64-22	5.5%	250	3.65	0.381	0.550
N100	PG64-22	5.5%	250	3.61	0.330	0.586

J. Eng. Mech., 2022, 148(2): 04021140

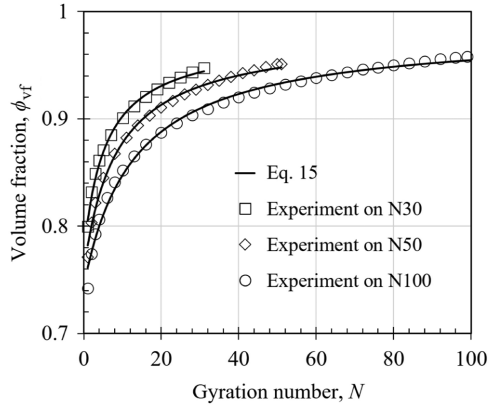

Fig. 8. Measured compaction curves and optimum fits by Eq. (16).

determined the theoretical maximum specific gravity, G_{mm}, based on ASTM D2041 (ASTM 2011). We used the recorded time history of the position of the bottom plate to calculate the time-dependent height of the mixture, $h_m(i)$, after an ith number of gyrations. By using the measured values of G_{mm} and G_{mb} and the height of the asphalt mixture, we calculated the time evolution of the volume fraction of the mixture as

$$\phi_{\text{vf}}(i) = \frac{G_{mb}}{G_{mm}} \frac{h_m^f}{h_m(i)} \tag{15}$$

where h_m^f = the height of the mixture measured at the end of the compaction test.

We compacted all three mixtures to a target volume fraction of 95%. The experimental results are shown in Fig. 8. The three mixes reached a 95% volume fraction at about 30, 50, 100 gyrations, and accordingly, we labeled these mixes as N30, N50, and N100. The result shows that ~80% of the total compaction deformation is achieved in the first 20 gyrations. The compaction rate gradually decreases as the number of gyration increases.

For these mixtures experiments, since we made all the mixtures using the same binder, we hypothesize that the difference in compaction behavior in our experiments was caused by the aggregate size distribution. Based on the information presented in Table 2, we hypothesize that the compaction efficiency improves with a decreased median size of fine aggregates and an increased mass portion of fine aggregates, α_f. We expect this might be because fine aggregates can fill the voids more easily than coarse aggregates and with the help of a fines-rich FAM. We may also expect that a larger portion of fine aggregates would allow a more effective compaction of the mixture, and the overall median size of aggregates would also affect the compaction efficiency. However, this effect is not studied here due to the availability of aggregates.

We compare our measured compaction curves with a semiempirical compaction model developed for relatively monodisperse granular assemblies under tapping excitations proposed by Knight et al. (1995). The model takes the following form

$$\phi_{vf}(t) = \phi_\infty - \frac{\phi_\infty - \phi_0}{1 + B\ln(1 + t/\tau_0)} \tag{16}$$

where ϕ_∞ =final volume fraction; and ϕ_0 = initial volume fraction of the mixture before the compaction test starts. Here we consider $\phi_\infty = 1$, and τ_0 and B are obtained by optimum fitting of the measured compaction curves. Fig. 8 shows that Eq. (16) can fit the data well, which we find interesting because the HMA is significantly different in particle shape and grain size distribution than the systems for which it was developed.

DEM Simulations of Gyratory Compaction

We now use our DEM to simulate the gyratory compaction experiments. As mentioned earlier, we explicitly model the motion of the coarse aggregates ($d > 2.36$ mm) based on the aggregate size distribution and represent the FAM using our granular-fluid rheology described in Section 3. In our DEM simulations, we determine the coating thickness of the coarse aggregates so that the total volume of the coating is equal to the volume of FAM. The coating thickness is used to determine δ_g in Eqs. (2*a*) and (2*b*).

Based on the aggregates we used in the experiments, we use the following particle properties, in our model: particle density $\rho_s = 2{,}650$ kg/m^3, elastic modulus of aggregates $E = 70$ GPa, and the Poisson's ratio $\nu = 0.20$. We calculate the damping coefficient for the Hertz–Mindlin contact forces based on $\alpha = 0.9$ (Table 1). According to (Foerster et al. 1994), we set the coefficient of friction between particles, $\mu_p = 0.10$. The particle size distribution follows the degradation curve of the aggregates shown in Fig. 7(b).

The lubrication interaction between particles is calculated based on the rheology of FAM represented by Eqs. (13) and (14). Though the range of particle size used in the simulation is considerably smaller than that actual particle size distribution of FAM, the rheology of granular mixture scales with the median grain size (Yohannes and Hill 2010). In the present rheology model, the median size of the fine aggregates is directly captured by the dimensionless number, K. To initiate each simulation, we generate approximately 1,000 particles with randomly assigned particles to match the size distribution of the coarse aggregates in the HMA mixture. We drop these particles into a tilted cylindrical chamber with random initial velocities so we obtain a randomly arranged initial state. The cylindrical chamber is tilted with an angle of 1.25°. We then add a top plate to the tilted chamber. We push the bottom plate upward at a constant pressure of 600 kPa, while we gyrate the top plate and the cylindrical ring in the same manner as the Superpave gyratory compactor so that the gyratory speed is 30 rpm. We perform the simulation with a small-time increment on the order of 10^{-8} seconds and at each time step calculate accelerations, velocities, and displacements using the forces and integrating according to the fourth-order Runge–Kutta method. Fig. 9 presents the snapshots of different stages of the DEM simulations.

During the simulation, the movement of the bottom plate is recorded, from which we can calculate the solid fraction of the mixture as

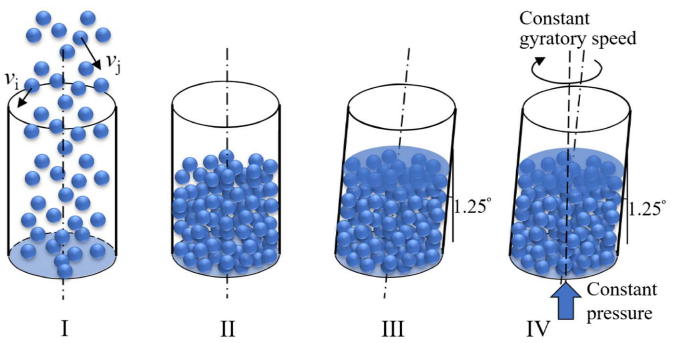

Fig. 9. Snapshots of different stages of DEM simulation of gyratory compaction of HMA.

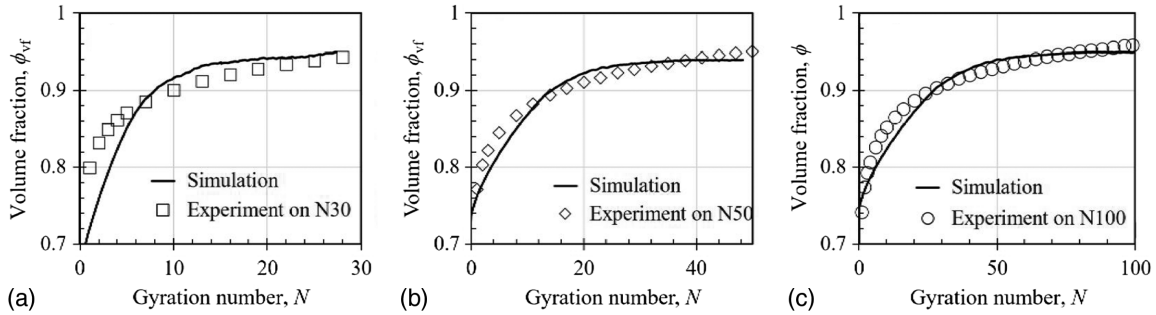

Fig. 10. Comparison between the measured and simulated compaction curves.

$$\phi_{vf}(t) = \frac{V_{ca} + V_{FAM}}{A_0 h(t)} \tag{17}$$

where $\phi_{vf}(t)$ = volume fraction of the asphalt mixture at time t; V_{ca} = volume of coarse aggregates; V_{FAM} = volume of FAM; A_0 = cross sectional area of the cylindrical gyratory ring in the simulation; and $h(t)$ = distance between the top and bottom plates measured at time t. We use Eq. (17) to obtain the relationship between ϕ_{vf} and gyration number.

Fig. 10 compares the simulated and measured compaction curves of all three mixtures. We can see that our simulations can predict the overall compaction behavior reasonably well. The simulation predicts that the mixture is quickly compacted in the first 20 gyrations, and the compaction rate decreases significantly as the solid fraction reaches 90%. More importantly, the present model is able to predict the pronounced difference in compaction efficiency for mix designs of different aggregate size distributions. This shows the main advantage of DEM, which can explicitly take into account the microstructural arrangements of the particles and the effects of changing grain size distributions on time-dependent compaction in response to arbitrary stresses. By contrast, continuum-based models are not yet able to predict the effect of aggregate size on the compaction behavior of asphalt mixtures.

We consider the main differences in three sets of aggregates used in the experiment (Table 2) are (1) the median size d_a of fine aggregates, and (2) the portion of fine aggregates represented by α_f. We note that as the compaction rate increases from the N100 system to the N50 system to the N30 system, d_a decreases monotonically and α_f increases monotonically. Through our smaller scale shear cell experiments, the median size of fine aggregates d_a directly affects the rheology of FAM [Eqs. (13) and (14)]. For two systems of different grain size distributions and the same η_f subjected to the same shear rate and normal stress, the one with a smaller value of d_a would have a smaller I_c, effective frictional coefficient [μ_{eff}, Eq. (10)], and effective shear viscosity [η_s, Eq. (13)]. The resulting decrease in the lubrication forces allows the coarse aggregates to move more easily and, subsequently, allows for compaction to progress more quickly. Additionally, a decrease in the effective frictional coefficient would make the particles less frictional and therefore enhance the particle rearrangement during compaction. This supports results from previous studies (Song et al. 2008) indicating that reducing an effective interparticle friction can give rise to better compaction and further demonstrates the particular physics of this lowered friction is associated with finer particles in the FAM (Srebro and Levine 2003).

An increase in the portion of fine aggregates, α_f, indicates there is a thicker coating of FAM on the surface of coarse aggregates. A thinner coating allows aggregates to more equally come into contact and to interlock with one another. A thicker coating limits this interlocking and facilitates aggregate movement past one another and, in response to applied stresses, faster compaction. To determine which is responsible for an increased compaction rate, a reduced d_a and/or an increased α_f, requires more frequent output of the data and associated interrogation of those data, a topic of future work.

Scrutiny of Fig. 10 shows that even though the simulation can capture well the overall behavior of the compaction process, the simulation result deviates from the experiment, particularly during the initial stage of the compaction. In every case, the model predicts slower compaction than exhibited by the experiments for the first several cycles. We suggest four things that future endeavors could address to significantly advance our understanding of these dynamics.

First, this deviation could be caused by the representation of nonsphericity of the composite particles, which may result in a different degree of particle interlocking than occurs in reality. If so, this could impede compaction rate more than is physically realistic during these early times. We hypothesize that the modeling of compaction during the first several cycles could be improved by choosing a lower value of nonsphericity of the composite particles or even a more detailed representation of the particles by using multiple spheres to represent each.

Second, we model the fine particles in the FAM as spheres in a relatively narrow distribution of sizes. These simplifications might limit the effectiveness of our representation of the FAM behavior and the derivation of its rheology for upscaling.

Third, our representation of the FAM-modified interparticle contacts involves what we might call a viscocollisional model that requires a few parameters to be fitted to experiments or 3-d simulations. To the authors' knowledge, there are no such existing data for the range of parameters we need for FAM, so we performed simulations for which the binder was represented as a relatively simple spherical shell coating and only lubrication forces were represented. A better representation could include a more complete range of fluid forces that include effects like drag and added mass. Along these lines, the theoretical viscocollisional model itself is a steady state model. There is no analogous model that can capture what is likely to be an evolving rheology of fluid out of equilibrium with its forcing conditions.

Fourth and lastly, our rheological model for FAM is implemented in the large-scale simulations through a coating framework similar to our small-scale simulations of the FAM. As such, we do not capture the inertial effects of the fluid itself like an added mass term or drag forces. A consideration of different up-scaled representations of this fluid may be more effective. Alternatively, one might consider a viscoelastic framework for the FAM, such as a

recently developed model, described in Ref. (Olsson et al. 2019). In this case, they consider a viscoelastic material (compared with our viscocollisional fluid) and model the interparticle FAM-mediated interaction in the normal direction using the theoretical work (Lee and Radok 1960) on the spherical indentation of a viscoelastic material.

Summary and Conclusions

To summarize, in this study, we developed a two-scale DEM for simulating gyratory compaction of HMA. The model explicitly represents the coarse aggregates by representing nonspherical particles using assemblies of two different sized spheres. It further represents the material properties of the particles and fluids using the Hertz–Mindlin contact and the lubrication interaction forces between the aggregates. To model the lubrication interaction, we show that it suffices to consider the effects of the constituents of FAM as viscoinertial fluids whose rheology captures the properties of the viscous fluid (asphalt binder) and the fine particles (fine aggregates). We demonstrated that the overall rheology of FAM can be captured using a previously developed expression for particle slurries, which we demonstrated by performing DEM simulations of simple shear tests and incorporating the results into a larger scale simulation of the compaction process itself.

The present computational model agrees well with the gyratory compaction experiments on three different particle size distributions in HMA's without any fitting parameters to represent the difference from one mixture to the next. This indicates a path for using DEM to capture the influence of particle properties and size distributions on the compaction of the hot mixed asphalt. Our results indicate that faster compaction behavior is highly correlated with a smaller median particle size in the FAM and a higher ratio of fine to coarse particle sizes.

The results of this study indicate that the DEM could provide a viable means to capturing the effects of the properties of constituents of HMA, such as binder viscosity and aggregate size distribution, on its compaction efficiency. To make this more fully viable requires a more detailed understanding of the specifics of aggregate shape and the relative importance of the size of fine particles and the quantity relative to coarse particles. Ultimately, these results could lead to a simulation-based mix design of asphalt mixtures for optimizing the compaction performance.

Data Availability Statement

All data and models that support the findings of this study are available from the corresponding author upon reasonable request.

Acknowledgments

The authors acknowledge the financial support from the Minnesota Department of Transportation through grant WO20 to the University of Minnesota (UMN) and from the Center of Transportation Studies at UMN and the computing resources provided by Saint Anthony Fall Laboratory at UMN. Hill gratefully acknowledges support for studying the rheology of particle-fluid mixtures from the National Science Foundation (NSF GLD-1451957). T. Man also gratefully acknowledges the Sommerfeld Fellowship provided by the Department of Civil, Environmental, and Geo-Engineering at UMN.

References

ASTM. 2011. *Standard test method for theoretical maximum specific gravity and density of bituminous paving mixtures*. ASTM D2041M-11. West Conshohocken, PA: ASTM.

ASTM. 2015. *Standard test method for preparation and determination of the relative density of asphalt mix specimens by means of the Superpave gyratory compactor*. ASTM D6925-15. West Conshohocken, PA: ASTM.

ASTM. 2019. *Standard test method for bulk specific gravity and density of non-absorptive compacted asphalt mixtures*. ASTM D2726-19. West Conshohocken, PA: ASTM.

Bagnold, R. A. 1954. "Experiments on a gravity-free dispersion of large solid spheres in a Newtonian fluid under shear." *Proc. R. Soc. London* 225 (1160): 49–63. https://doi.org/10.1098/rspa.1954.0186.

Boyer, F., É. Guazzelli, and O. Pouliquen. 2011. "Unifying suspension and granular rheology." *Phys. Rev. Lett.* 107 (18): 188301. https://doi.org/10.1103/PhysRevLett.107.188301.

Caro, S., E. Masad, A. Bhasin, and D. Little. 2010. "Micromechanical modeling of the influence of material properties on moisture-induced damage in asphalt mixtures." *Constr. Build. Mater.* 24 (7): 1184–1192. https://doi.org/10.1016/j.conbuildmat.2009.12.022.

Cassar, C., M. Nicolas, and O. Pouliquen. 2005. "Submarine granular flows down inclined planes." *Phys. Fluids* 17 (10): 103301. https://doi.org/10.1063/1.2069864.

Chen, J., B. Huang, and X. Shu. 2012. "Air-void distribution analysis of asphalt mixture using discrete element method." *J. Mater. Civ. Eng.* 25 (10): 1375–1385. https://doi.org/10.1061/(ASCE)MT.1943-5533.0000661.

Chen, J., B. Huang, X. Shu, and C. Hu. 2014. "Dem simulation of laboratory compaction of asphalt mixtures using an open source code." *J. Mater. Civ. Eng.* 27 (3): 04014130. https://doi.org/10.1061/(ASCE)MT.1943-5533.0001069.

Foerster, S. F., M. Y. Louge, H. Chang, and K. Allia. 1994. "Measurements of the collision properties of small spheres." *Phys. Fluids* 6 (3): 1108–1115. https://doi.org/10.1063/1.868282.

Forterre, Y., and O. Pouliquen. 2008. "Flows of dense granular media." *Annu. Rev. Fluid Mech.* 40 (1): 1–24. https://doi.org/10.1146/annurev.fluid.40.111406.102142.

Goldman, A. J., R. G. Cox, and H. Brenner. 1967. "Slow viscous motion of a sphere parallel to a plane wall–i motion through a quiescent fluid." *Chem. Eng. Sci.* 22 (4): 637–651. https://doi.org/10.1016/0009-2509(67)80047-2.

Graziani, A., S. Raschia, C. Mignini, A. Carter, and D. Perraton. 2020. "Use of fine aggregate matrix to analyze the rheological behavior of cold recycled materials." *Mater. Struct.* 53 (4): 1–16. https://doi.org/10.1617/s11527-020-01515-7.

Guler, M., P. J. Bosscher, and M. E. Plesha. 2004. "A porous elasto-plastic compaction model for asphalt mixtures with parameter estimation algorithm." In *Recent advances in materials characterization and modeling of pavement systems*, 126–143. Reston, VA: ASCE.

Hartley, R., and R. Behringer. 2003. "Logarithmic rate dependence of force networks in sheared granular materials." *Nature* 421 (6926): 928. https://doi.org/10.1038/nature01394.

Hill, K. M., and D. S. Tan. 2014. "Segregation in dense sheared flows: Gravity, temperature gradients, and stress partitioning." *J. Fluid Mech.* 756 (Oct): 54–88. https://doi.org/10.1017/jfm.2014.271.

Jop, P., Y. Forterre, and O. Pouliquen. 2006. "A constitutive law for dense granular flows." *Nature* 441 (7094): 727. https://doi.org/10.1038/nature04801.

Knight, J. B., C. G. Fandrich, C. N. Lau, H. M. Jaeger, and S. R. Nagel. 1995. "Density relaxation in a vibrated granular material." *Phys. Rev. E* 51 (5): 3957. https://doi.org/10.1103/PhysRevE.51.3957.

Koneru, S., E. Masad, and K. Rajagopal. 2008. "A thermomechanical framework for modeling the compaction of asphalt mixes." *Mech. Mater.* 40 (10): 846–864. https://doi.org/10.1016/j.mechmat.2008.03.008.

Le, J.-L., R. Hendrickson, M. O. Marasteanu, and M. Turos. 2018. "Use of fine aggregate matrix for computational modeling of low temperature fracture of asphalt concrete." *Mater. Struct.* 51 (6): 152. https://doi.org/10.1617/s11527-018-1277-x.

Le, J.-L., M. O. Marasteanu, and M. Turos. 2020. "Mechanical and compaction properties of graphite nanoplatelet-modified asphalt binders and mixtures." *Road Mater. Pavement Des.* 21 (7): 1799–1814. https://doi.org/10.1080/14680629.2019.1567376.

Lee, E., and J. R. M. Radok. 1960. "The contact problem for viscoelastic bodies." *J. Appl. Mech.* 27 (3): 438–444. https://doi.org/10.1115/1.3644020.

Liu, P., R. Yang, and A. Yu. 2013. "Dem study of the transverse mixing of wet particles in rotating drums." *Chem. Eng. Sci.* 86 (Feb): 99–107. https://doi.org/10.1016/j.ces.2012.06.015.

Luding, S., M. Nicolas, and O. Pouliquen. 2000. "A minimal model for slow dynamics: Compaction of granular media under vibration or shear." In *Compaction of soils, granulates and powders*, 241–249. Rotterdam, Netherlands: A.A. Balkema.

Man, T. 2019. "Rheology of granular-fluid systems and its application in the compaction of asphalt mixtures." Ph.D. thesis, Dept. of Civil Engineering, Univ. of Minnesota. https://hdl.handle.net/11299/202919.

Marshall, J. S., and S. Li. 2014. *Adhesive particle flow*. Cambridge, UK: Cambridge University Press.

Masad, E., A. Scarpas, A. Alipour, K. R. Rajagopal, and C. Kasbergen. 2016a. "Finite element modelling of field compaction of hot mix asphalt. Part I: Theory." *Int. J. Pavement Eng.* 17 (1): 13–23. https://doi.org/10.1080/10298436.2013.863309.

Masad, E., A. Scarpas, K. R. Rajagopal, E. Kassem, S. Koneru, and C. Kasbergen. 2016b. "Finite element modelling of field compaction of hot mix asphalt. Part II: Applications." *Int. J. Pavement Eng.* 17 (1): 24–38. https://doi.org/10.1080/10298436.2013.863310.

Mehta, A., G. Barker, and J. Luck. 2004. "Cooperativity in sandpiles: Statistics of bridge geometries." *J. Stat. Mech: Theory Exp.* 2004 (10): P10014. https://doi.org/10.1088/1742-5468/2004/10/P10014.

MiDi, G. 2004. "On dense granular flows." *Eur. Phys. J.* 14 (4): 341–365. https://doi.org/10.1140/epje/i2003-10153-0.

Nicolas, M., P. Duru, and O. Pouliquen. 2000. "Compaction of a granular material under cyclic shear." *Eur. Phys. J.* 3 (4): 309–314. https://doi.org/10.1007/s101890070001.

Nowak, E. R., J. B. Knight, E. Ben-Naim, H. M. Jaeger, and S. R. Nagel. 1998. "Density fluctuations in vibrated granular materials." *Phys. Rev. E* 57 (2): 1971. https://doi.org/10.1103/PhysRevE.57.1971.

Olsson, E., D. Jelagin, and M. N. Partl. 2019. "New discrete element framework for modelling asphalt compaction." *Road Mater. Pavement Des.* 20 (2): 604–616. https://doi.org/10.1080/14680629.2019.1633750.

Peng, G., and T. Ohta. 1998. "Logarithmic density relaxation in compaction of granular materials." *Phys. Rev.* 57 (1): 829. https://doi.org/10.1103/PhysRevE.57.829.

Pitois, O., P. Moucheront, and X. Chateau. 2000. "Liquid bridge between two moving spheres: An experimental study of viscosity effects." *J. Colloid Interface Sci.* 231 (1): 26–31. https://doi.org/10.1006/jcis.2000.7096.

Pöschel, T., and T. Schwager. 2005. *Computational granular dynamics: Models and algorithms*. Berlin: Springer.

Pouliquen, O., M. Belzons, and M. Nicolas. 2003. "Fluctuating particle motion during shear induced granular compaction." *Phys. Rev. Lett.* 91 (1): 014301. https://doi.org/10.1103/PhysRevLett.91.014301.

Pouliquen, O., C. Cassar, P. Jop, Y. Forterre, and M. Nicolas. 2006. "Flow of dense granular material: Towards simple constitutive laws." *J. Stat. Mech: Theory Exp.* 2006 (7): P07020. https://doi.org/10.1088/1742-5468/2006/07/P07020.

Ricardo-Archilla, A., and S. Madanat. 2001. "Statistical model of pavement rutting in asphalt concrete mixes." *Transp. Res. Rec.* 1764 (1): 70–77. https://doi.org/10.3141/1764-08.

Song, C., P. Wang, and H. A. Makse. 2008. "A phase diagram for jammed matter." *Nature* 453 (7195): 629–632. https://doi.org/10.1038/nature06981.

Srebro, Y., and D. Levine. 2003. "Role of friction in compaction and segregation of granular materials." *Phys. Rev. E* 68 (6): 061301. https://doi.org/10.1103/PhysRevE.68.061301.

Trulsson, M., B. Andreotti, and P. Claudin. 2012. "Transition from the viscous to inertial regime in dense suspensions." *Phys. Rev. Lett.* 109 (11): 118305. https://doi.org/10.1103/PhysRevLett.109.118305.

Tsuji, Y., T. Tanaka, and T. Ishida. 1992. "Lagrangian numerical simulation of plug flow of cohesionless particles in a horizontal pipe." *Powder Technol.* 71 (3): 239–250. https://doi.org/10.1016/0032-5910(92)88030-L.

Wang, L., B. Zhang, D. Wang, and Z. Yue. 2007. "Fundamental mechanics of asphalt compaction through fem and DEM modeling." In *Analysis of asphalt pavement materials and systems: Engineering methods*, 45–63. Reston, VA: ASCE.

Yohannes, B., and K. Hill. 2010. "Rheology of dense granular mixtures: Particle-size distributions, boundary conditions, and collisional time scales." *Phys. Rev. E* 82 (6): 061301. https://doi.org/10.1103/PhysRevE.82.061301.

Zhao, T., F. Dai, N. Xu, Y. Liu, and Y. Xu. 2015. "A composite particle model for non-spherical particles in dem simulations." *Granular Matter* 17 (6): 763–774. https://doi.org/10.1007/s10035-015-0596-7.